Hindawi Publishing Corporation
Advances in OptoElectronics
Volume 2012, Article ID 482074, 10 pages
doi:10.1155/2012/482074

Research Article

Substitution of Ethynyl-Thiophene Chromophores on Ruthenium Sensitizers: Influence on Thermal and Photovoltaic Performance of Dye-Sensitized Solar Cells

Malapaka Chandrasekharam,[1] Ganugula Rajkumar,[2] Thogiti Suresh,[1] and Paidi Yella Reddy[2]

[1] *Inorganic and Physical Chemistry Division, Indian Institute of Chemical Technology, Uppal Road, Tarnaka, Hyderabad 500 607, India*
[2] *Aisin Cosmos R&D Co. Ltd, Indian Institute of Chemical Technology, Uppal Road, Tarnaka, Hyderabad 500 607, India*

Correspondence should be addressed to Malapaka Chandrasekharam, csmalapaka@yahoo.com

Received 30 April 2011; Accepted 10 October 2011

Academic Editor: Surya Prakash Singh

A new high molar extinction coefficient ruthenium(II) bipyridyl complex, "Ru(2,2-bipyridine-4,4′-dicarboxylic acid)(4,4′-bis((3-hexylthiophen-2-yl)ethynyl)-2,2′-bipyridine)$(NCS)_2$ $(N(C_4H_9)_4)$, **MC**101" was synthesized and fully characterized by ^{1}H-NMR, ESI-MASS, FT-IR, UV-Vis., and fluorescence spectroscopes. The dye showed relatively high molar extinction coefficient of $25.0 \times 10^3\,M^{-1}\,cm^{-1}$ at λ maximum of 544 nm, while the reference **C**101 has shown $15.8 \times 10^3\,M^{-1}cm^{-1}$ at λ maximum 528 nm. The monochromatic incident photon-to-collected electron conversion efficiency of 44.1% was obtained for **MC**101 over the entire visible range, while the **C**101 sensitized solar cell fabricated and evaluated under identical conditions exhibited 40.1%. The DSSCs fabricated with 0.54 cm^2 active area TiO_2 electrodes and high efficient electrolyte (**E**01), from the sensitizers **MC**101 and **C**101 exhibited energy conversion efficiencies of 3.25% (short-circuit current density (J_{SC}) = 7.32 mA/cm^2, V_{OC} = 610 mV, ff = 0.725) and 2.94% (J_{SC} = 6.60 mA/cm^2; V_{OC} = 630 mV; ff = 0.709), respectively, under air mass of 1.5 sunlight.

1. Introduction

Photovoltaic (PV) cells generating clean electricity are now getting ready for significant market expansion in this new millennium, as the solar energy is the major renewable energy source and the major alternative to the fast depleting and polluting fossil fuels [1]. In the past decades, low-cost excitonic solar cells attracted worldwide attention among academic and industrial players as potential candidates for the future PV market [2]. Among this class of organic photovoltaics, the mesoscopic dye-sensitized solar cell [3–5] (DSSC) has achieved a respectable high-efficiency [6, 7] and a remarkable stability under the prolonged thermal and light-soaking dual stress [8–12]. The record efficiency of ~11% [6, 7] in DSSCs measured under the air mass 1.5 global (AM 1.5 G) illumination is achieved with the well-known **N**719 sensitizer employing a volatile acetonitrile-based electrolyte. However, stability under prolonged heating at 80°C has proved too hard to reach with the high-efficiency **N**719-based cells. In 2003, a thermally stable, ~7% efficiency DSSC [9] was disclosed, employing the amphiphilic **Z**907 sensitizer [8] and a 3-methoxypropionitrile-(MPN-) based electrolyte avoiding lithium salts as additives. However, the molar extinction coefficient of this sensitizer is somewhat lower than that of the standard **N**719 dye. Meanwhile, a compromise between efficiency and high temperature stability has been noted for the **Z**907 sensitizer [13]. For commercial applications of DSSCs, it is necessary to employ nonvolatile or even solvent-free electrolytes. However, with a low-fluidity electrolyte, the charge collection yield becomes low due to the shortened electron diffusion length. Enhancing the optical absorptivity of a stained mesoporous film can counter this effect. Thus, Wang et al. initiated the concept of developing high molar extinction coefficient, amphiphilic ruthenium sensitizer, [14] followed by other groups, [15–20] with a motivation to enhance device efficiency of DSSCs. In

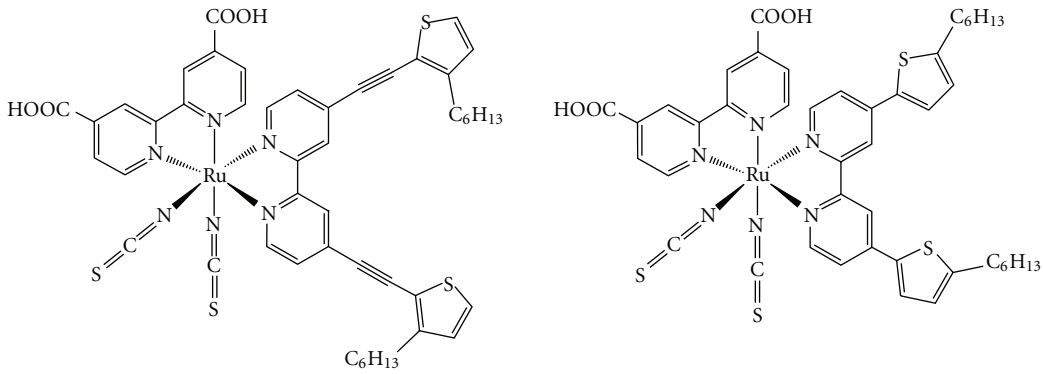

Figure 1: Structure of new ruthenium(II) complex, **MC**101 and reference **C**101 sensitizers.

this context, sensitizers such as **K**19 [10, 11] and its analogue **K**77 [12] have been successfully developed to fabricate thermally stable DSSCs showing ~8 and ~8.5% initial efficiencies, respectively.

The sensitizer **C**101 with a molar extinction coefficient of $15.7 \times 10^3\,M^{-1}\,cm^{-1}$ demonstrated benchmarks under the illumination of AM 1.5 G full sunlight, such as a 11.0% efficiency along with an acetonitrile-based electrolyte, a long-term stable >9% device using a low volatility electrolyte, and a long-term stable 7.4% device employing an ionic liquid electrolyte [20]. Chen et al. [19] communicated a similar sensitizer like **C**101 with a molar extinction coefficient of $15.7 \times 103\,M^{-1}\,cm^{-1}$, showing an efficiency of 7.39% with a highly volatile acetonitrile-based electrolyte.

As a part of our ongoing programme on the development of various metal free organic, phthalocyanine, and ruthenium sensitizers for applications in DSSCs [21–26], we recently reported a new record high efficiency DSSC using novel coadsorbents [27]. In this paper, we present a new promising sensitizer, coded **MC**101 (Figure 1) wherein the ancillary ligand, 4,4′-bis(5-hexylthiophen-2-yl)-2,2′-bipyridine (**L**2), of **C**101 is replaced with 4,4′-bis((3-hexylthiophen-2-yl)ethynyl)-2,2′-bipyridine (**L**1). The alkynyl thiophene group incorporates increased conjugation in the ancillary ligand, as the triple bond conjugated to double bonds (in the thiophene moiety) in order to achieve a higher molar extinction coefficient. The electron transfer is expected to be faster in this ligand due to the linear nature of alkynyl group and hence more stable than the isomerization (*cis-trans*) prone double bonds. We describe the synthesis and complete characterization of **MC**101 sensitizer and the photovoltaic performance of DSSC of **MC**101 in combination with high efficiency (**E**01) electrolyte. The photovoltaic characteristics were compared with that of **C**101.

2. Results

2.1. Synthesis and Characterization. All solvents and reagents, unless otherwise stated, were of Laboratory Reagent Grade and used as received. Brucker 300 Avance ^{1}H-NMR spectrometer run at 500 MHz was employed to record the ^{1}H NMR spectrum. Shimadzu LCMS-2010EV model with ESI probe was employed for MASS analysis. Shimadzu UV-Vis spectrometer (model 1700) and Fluorolog 3, J.Y.Horiba Fluorescence spectrometer were employed to record the electronic absorption and emission spectra. The 4,4′-dibromo-2,2′-bipyrdine, procured from Heterocycles and Catalysts, Gundeldingerstrasse 174, CH-4053 Basel, Switzerland, was used as received. The 3-bromo-thiophene, procured from Sigma-Aldrich.

The series of steps involved in the synthesis of **MC**101 are shown in Scheme 1. Initially the sonogashira reaction of 4,4′-dibromo-2,2′-bipyrdine with TIPS acetylene in presence of Pd(II) catalyst resulted in formation of 4,4′-bis((triisopropylsilyl)ethynyl)-2,2′-bipyridine (**1**), which was further protonated with TBAF to afford 4,4′-bis((triisopropylsilyl)ethynyl)-2,2′-bipyridine (**2**). The Grignard reagent 3-thienyl magnesium bromide prepared from 3-bromo thiophene on treatment with Mg followed by reaction with 4-bromo-hexane resulted in formation of 3-hexyl-thiophene (**3**), which on further treatment with elemental iodine provided 2-iodo-3-hexyl-thiophene (**4**). The sonogashira reaction of the alkyne **2** with the iodo compound **4** under Pd(II) conditions result in formation of 4,4′-bis [(3-hexyl thiophene)ethynyl]-2,2′-bipyridine (**L1**). The reaction of **L**1 with dichloro (*p*-cymene) ruthenium(II) dimer in presence of refluxing DMF afforded chloro (*p*-cymene) ruthenium bipyridyl complex intermediate, which on further reaction with 2,2′-bipyridine-4,4′-dicarboxylic acid in presence of excess NH_4NCS resulted in formation of **MC**101 complex. The crude compound was purified on Sephadex LH-20 column chromatography.

2.1.1. Synthesis of 4,4′-bis(triisopropylsilylacetylene)2,2′-bipyridin(1). A solution of 4,4′-dibromo-2,2′-bipyridine (1.000 g, 3.184 mmol), bis(triphenylphosphine)palladium(II) chloride (0.090 g, 0.127 mmol), copper(I) iodide (0.037 g, 0.197 mmol), and triisopropylsilyl acetylene (3.10 mL, 13.93 mmol) in triethylamine (10 mL) was heated in a sealed tube at 100°C for 20 hours. The mixture was washed with water, brine solution, and the organic compound was extracted in dichloromethane. The organic layer

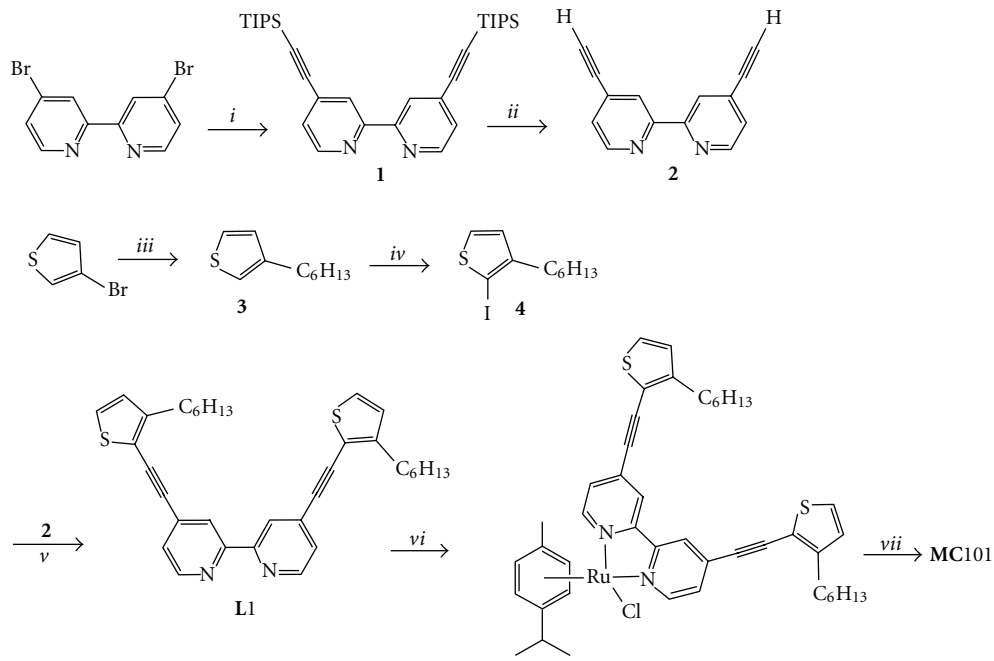

Scheme 1: Synthesis route for **MC**101 sensitizer, (*i*) TIPS acetylene, $Pd(PPh_3)Cl_2$, CuI, TEA, 100°C, 20 hours, 80%, (*ii*) TBAF, THF, 12 hours, RT, 65%, (*iii*) Mg, $C_6H_{13}Br$, ether, RT, 5 hours, 90%; (*iv*) I_2, HgO, ether, RT, 1 hour, 80%, (*v*) TEA, THF, $Pd(PPh_3)_2Cl_2$, CuI, 70°C, 24 hours, 80%, (*vi*) a. Ru-*p*-cymene complex, DMF, 60–70°C, 4 hours, b. 2,2′-bipyridine-4,4′-dicarboxylic acid, NH_4NCS, DMF, reflux, 8 hours 60%.

was then dried over sodium sulfate, and the solvent was evaporated under vacuum. The crude product was then purified by column chromatography (silica gel) using hexane/ethyl acetate (96/4 v/v) as eluent to afford **1** (1.310 g, 80%). ^{1}H NMR ($CDCl_3$, 25°C, 500 MHz) δ: 1.15 (s, 42H), 7.31 (d, 2H), 8.43 (s, 2H), and 8.6 (d, 2H). Chemical formula $C_{32}H_{48}N_2Si_2$: ESI-MS: Calcd for $(M+H)^+$: 517, found: 517 (100%).

2.1.2. Synthesis of 4,4′-bis(acetylene)-2,2′-bipyridine (2). 4,4′-bis(triisopropylsilylacetylene)-2,2′-bipyridine (0.894 g, 2.52 mmol) was taken in dry THF (15 mL) and added a solution of tetrabutylammonium fluoride (2.6 mL, 5.04 mmol) under nitrogen atmosphere. The reaction mixture was stirred for 12 hours at room temperature, extracted with ethyl acetate and washed with brine solution. The organic layer was dried over sodium sulfate before drying over vacuum. The crude compound was then purified over column chromatography (silica gel) using hexane/ethyl acetate (95/5 v/v) as eluent (0.229 g, 65%). ^{1}H NMR ($CDCl_3$, 25°C, 300 MHz) δ: 3.32 (s, 2H), 7.38 (dd, 2H), 8.48 (s, 2H), 8.66 (d, 2H). Chemical formula $C_{14}H_8N_2$: ESI-MS: Calcd for $(M+H)^+$: 205, found: 205 (100%).

2.1.3. Synthesis of 3-hexylthiophene (3). Mg (0.208 g, 8.58 mmol) was suspended in dry diethyl ether (15 mL) at 0°C under nitrogen atmosphere. To this suspension, a solution of 1-bromohexane (1.03 mL, 7.35 mmol) in diethyl ether (5 mL) was added drop wise and the mixture stirred at room temperature for 2 hours then Grignard reagent thus obtained was added in portions to a solution of 3-bromothiophene (1.000 g, 6.13 mmol) and $[NiCl_2(dppp)_2]$ (0.07 mg, 0.12 mmol) in diethyl ether and the mixture stirred for another 3 hours at room temperature. The reaction mixture was then quenched with water, the organic layer separated, and the aqueous layer extracted with diethyl ether. The combined organic layers were dried over sodium sulfate and the solvent removed under reduced pressure. The crude compound was purified by column chromatography (silica gel) eluting with hexane to give yellow oil (0.926 g, 90%). ^{1}H NMR ($CDCl_3$, 25°C, 300 MHz) δ: 0.89 (t, 3H), 1.31 (m, 6H), 1.62 (q, 6H), 2.62 (t, 2H), 6.92 (d, 1H), 6.95 (d, 1H), and 7.24 (dd, 1H). Chemical formula $C_{10}H_{16}S$: ESI-MS: Calcd for $(M+H)^+$: 169, found: 169 (100%).

2.1.4. Synthesis of 3-Hexyl-2-iodothiophene (4). To a solution of 3-hexylthiophene (1.000 g, 5.95 mmol) in toluene was added HgO (1.290 g, 5.95 mmol) and iodine (1.511 g, 5.95 mmol) in portions over 30 minutes at 0°C. The reaction mixture was stirred at room temperature for 1 hour. The purple color changes to orange color, then the orange precipitate was filtered off and washed two times with diethyl ether. The organic layers were combined and washed with aqueous sodium thiosulfate to remove excess iodine. The organic layer was separated and dried over sodium sulfate, and the solvent was removed under reduced pressure. The crude compound was purified on column chromatography (silica gel) using hexane as eluent to get the desired compound as colourless liquid (1.390 g, 80%). ^{1}H NMR ($CDCl_3$, 25°C, 300 MHz) δ: 0.89 (t, 3H), 1.31 (m, 6H), 1.56 (q, 2H), 2.55 (t, 2H), 6.75

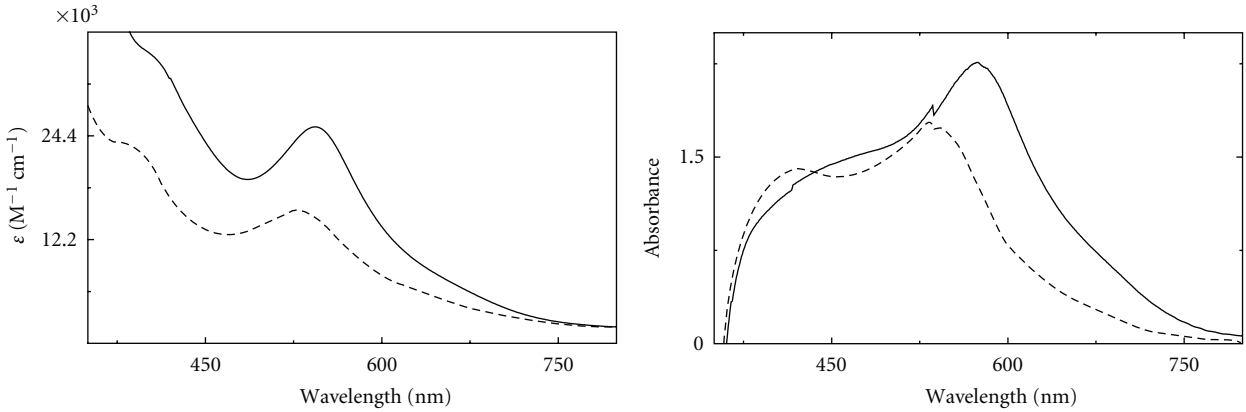

Figure 2: Equi-molar absorption spectra of **MC**101 (—) relative to reference **C**101 (- - -) (a) in ethanol and (b) over TiO_2 films.

(d, 1H), and 7.38 (d, 1H). Chemical formula $C_{10}H_{15}IS$: ESI-MS: Calcd for $(M+H)^+$: 295, found: 295 (40%).

2.1.5. Synthesis of 4,4′-Bis[(3-hexyl thiophene)ethynyl]-2,2′-bipyridine (5). A sealed tube is charged with 4,4′-bis (acetylene)-2,2′-bipyridine (0.200 g, 0.98 mmol), 3-hexyl-2-iodothiophene (0.632 mg, 2.15 mmol), bis(triphenylphosphine) palladium(II) chloride (0.014 g, 0.03 mmol), and copper(I) iodide (0.008 mg, 0.04 mmol) with degassed solvents triethylamine (10 mL) and THF (10 mL). The yellow solution was heated at 70°C for 24 hours, and then the solvent was evaporated on vacuum. The residue was treated with water and extracted with dichloromethane. The organic extracts were washed with water then brine and dried over sodium sulfate. The solvent was removed by rotary evaporation and the residue was purified by column chromatography on neutral alumina, eluting with dichloromethane/hexane (15/85 v/v) as eluent to get light yellow solid (0.420 g, 80%). ^{1}H NMR ($CDCl_3$, 25°C, 300 MHz) δ: 0.88 (t, 6H), 1.35 (m, 12H), 1.67 (q, 4H), 2.79 (t, 4H), 6.92 (d, 2H), 7.28 (d, 2H), 7.38 (dd, 2H), 8.48 (s, 2H), and 8.66 (d, 2H). Chemical formula $C_{34}H_{36}N_2S_2$: ESI-MS: Calcd for $(M+H)^+$: 537, found: 537 (100%).

*2.1.6. Synthesis of Ruthenium (II) Complex **MC**101.* 4,4′-bis [(3-hexylthiophene)ethynyl]-2,2′-bipyridine (0.085 g, 0.163 mmol) and dichloro(p-cymene)ruthenium(II) dimer (0.050 g, 0.082 mmol) in dry DMF were heated at 60°C for a period of 4 hours under argon in the dark. Subsequently, 4,4′′-dicarboxylic acid-2,2′-bipyridine (0.040 g, 0.163 mmol) was added and the reaction mixture was heated to 140°C for another 4 hours. To the resulting dark green solution was added NH_4NCS (0.193 g, 2.53 mmol) in water (2 mL), and the reaction mixture was further heated for 3 hours at 150°C. DMF was removed on rotoevaporatour under high vacuum, and water (250 mL) was added to get the precipitate. The solid was filtered off, washed with water and diethyl ether, and dried under vacuum. The crude compound was dissolved in methanol and dichloromethane and further purified on the sephadex LH-20 with methanol/dichloromethane (60/40 v/v) as eluent about three times to get pure **MC**101 as dark brown solid (0.090 g, 60%). ^{1}H NMR ($CDCl_3$, 25°C, 300 MHz) δ: 0.42 (t, 6H), 0.92 (m, 12H), 1.26 (q, 4H), 2.5 (t, 4H), 6.54 (d, 1H), 6.57 (d, 1H), 6.61 (d, 1H), 6.93 (d, 1H), 6.99 (d, 1H), 7.07 (d, 1H), 7.17 (d, 1H), 7.2 (d, 1H), 7.31 (d, 1H), 7.62 (d, 1H), 7.82 (s, 1H), 7.93 (s, 1H), 8.35 (s, 1H), 8.49 (s, 1H), 8.92 (d, 1H), 9.15 (d, 1H). Chemical formula $C_{60}H_{52}N_6O_4RuS_4$: ESI-MS: Calcd for $(M+H)^+$: 999, found: 999 (75%).

2.2. Absorption, Emission, and Electrochemical Properties. The electronic absorption spectrum of **MC**101 was recorded in ethanol and was compared with that of reference **C**101 (Figure 2(a)). The new sensitizer showed one intense absorption band at 544 nm, which is assigned to the metal to-ligand charge transition, and a relatively high intensity shoulder-type absorption band was observed at 410 nm. **MC**101 sensitizer showed molar extinction coefficient of 25,000 $M^{-1}cm^{-1}$ at λ maximum of 544 nm, while the reference **C**101 has shown 15,800 $M^{-1}cm^{-1}$ at λ maximum of 528 nm under comparable conditions. As compared to **C**101, the new sensitizer showed increased molar extinction coefficient with bathochromic shift in the absorption spectrum by 16 nm. The introduction of –C≡C– bonds through 4,4′-bis [(3-hexyl thiophene)ethynyl]-2,2′-bipyridine (**L**1) in **MC**101 complex exhibits high light harvesting ability as compared to 4,4′-bis(5-hexylthiophen-2-yl)-2,2′-bipyridine (**L**2) in **C**101 sensitizer by enhancing their molar extinction coefficient and by shifting the absorption spectrum towards IR region, which could be the contribution of extended –C≡C– of **L1** relative to **L2** [25–26]. Incorporation of alkyl thiophenes conjugated with bipyridine through –C≡C– into the ruthenium(II) pyridyl complex act as electron donor and consequently on excitation of the sensitizer, a faster charge transfer from HOMO to LUMO could be expected.

Besides the molar extinction coefficient and the absorption range, the size and geometrical structure of the sensitizer also influence the photovoltaic performance of DSSC. In order to see the quantity of the new sensitizer absorbed

on TiO_2 films relative to **C**101 sensitizer, the absorption measurements over TiO_2 films were carried out by staining 7 μm thick TiO_2 electrodes in 0.3 mM dye solutions prepared in ethanol (Figure 2(b)). Prior to cooling the TiO_2 electrodes, the dye solutions are sonicated for 10–15 minutes, and then TiO_2 electrodes, at around 100°C, are immersed into the dye solutions and allowed to soak for 16 hours under the dark. After that the electrodes were washed with ethanol to remove unadsorbed dye molecules and dried under nitrogen purging. As compared to **C**101, the new sensitizer is expected to show little lower film absorption over TiO_2 films due to its relatively larger size of the dye molecule, and the absorption measurements over TiO_2 films showed relatively increased film absorption for **MC**101 as compared to **C**101. To compare the anchoring pattern and surface morphology of the new sensitizer, the absorbance maxima of low energy absorption band of **MC**101 sensitizer are normalized by the corresponding absorbance maxima of **C**101, while their molar extinction coefficients are normalized by the molar extinction coefficient of **C**101. The film absorbance ratio of **MC**101 sensitizer calculated is lower than that of **C**101 indicating its lower packing density of the dye molecules on TiO_2 surface relative to **C**101. As expected, the lowest packing density of these sensitizers could be probably due to relatively little larger molecular diameter.

The cyclic voltammetry measurements of the new sensitizer was conducted to ensure that the LUMO of the new complex is suitable for injecting electrons into the conduction band of TiO_2 and also whether their HOMOs match the energy level of the I_2/I_3^- redox couple. The cyclic voltammogram of the dye was measured using tetrabutyl ammonium perchlorate (0.1 M in acetonitrile) as an electrolyte and ferrocene as an internal standard at 0.42 V versus SCE. Figure 3 shows the voltammogram of **MC**101 dye in acetonitrile**.** Reversible redox was observed for the sensitizer, similar to other ruthenium(II) pyridyl complexes [28]. The measured oxidation and reduction potentials are 0.820 and −0.80 V, respectively. The more positive potential of the sensitizer, relative to I^-/I_3^- redox couple (0.24 V versus SCE) in the electrolyte, provides a large thermodynamic driving force for the regeneration of the dye by iodide. Based on the absorption and emission spectra of the complex, the excitation transition energy (E_{0-0}) is estimated to be 1.957 (obtained by converting the wavelengths of 634 nm, at which their individual absorption and emission spectra intersect, into electron volts). The standard potential ($\phi^0(S^+/S^*)$) calculated from the relation of $[\phi^0(S^+/S) = \phi^0(S^+/S^*) - E_{0-0}]$ is −1.130 V versus SCE. So, $\phi^0(S^+/S^*)$ value is more negative (or higher in energy) than the conduction band edge of TiO_2 (−0.8 V versus SCE) providing ample thermodynamic driving force to inject electrons from the dye to TiO_2.

2.3. Computational Studies. The electronic ground-states of fully protonated **MC**101 was optimized in gaseous phase by using the Density Functional Theory (DFT) with MPW1PW91 method and lanl2dz basis set for ruthenium and 6–31G(d) for H, C, N, O, S atoms as implemented in Gaussian 09W and Gaussian View 5 interface software

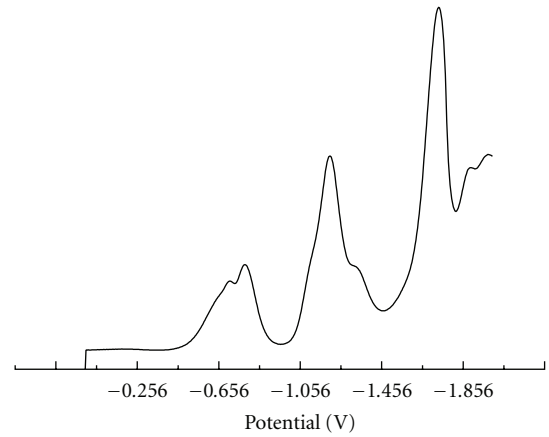

Figure 3: Differential pulse voltammograms of **MC**101 dye. Supporting electrolyte is 0.1 M tetrabutylammonium perchlorate in acetonitrile.

[29, 30]. Under identical conditions, the reference **C**101 was also optimized to compare electronic distribution in unoccupied and occupied frontier molecular orbitals. In order to see the influence of the ancillary bipyridine ligands 4,4′-bis((3-hexylthiophen-2-yl)ethynyl)-2,2′-bipyridine (**L**1) relative to 4,4′-bis(5-hexylthiophen-2-yl)-2,2′-bipyridine (**L**2) on optoelectronic properties of the corresponding ruthenium(II) complexes, the geometrical optimization of the electronic ground-states of **L**1 and **L**2 was also studied. Isodensity surface values are fixed at 0.04 for ruthenium(II) complexes, while for the ancillary ligands, the isodensity surface values are fixed at 0.02. The occupied (HOMO to HOMO-4) and unoccupied (LUMO to LUMO+4) frontier orbitals of **L**1 are shown in Figure 4. The HOMO and HOMO-1 orbitals of **L1** are degenerate and have $\boldsymbol{\pi}$-orbitals over bipyridine moiety and thiophen-2-yl, while in HOMO-2 orbital, the π-orbitals are almost localized on bipyridine. The HOMO-3 and HOMO-4 orbitals are again degenerate and the π-orbitals are localized over thiophene moieties. In case of LUMO and LUMO+1 orbitals of **L**1, the π^*-orbitals are delocalized over π-system with maximum components on the bipyridine, which depresses their energy levels relative to those of **L**2. In case of LUMO+3 and LUMO+4, $\boldsymbol{\pi}^*$-orbitals are localized on bipyridine and thiophen-2-yl.

The electronic distributions in unoccupied and occupied frontier molecular orbitals of **MC**101 are shown in Figure 5, while the corresponding orbitals of **C**101 calculated under similar conditions are shown in Figure 6. As expected, the first highest occupied molecular orbital (HOMO) of **MC**101 exhibits ruthenium *t*2g character with size mixing from thiocyanate ligand, while π-clouds for other HOMO-1 and HOMO-2 orbitals are considered with size mixing from one of thiocyanate ligands. In case of **C**101, the first three occupied (HOMO to HOMO-2) orbitals follow t2g character with size mixing from thiocyanate ligand. The π-clouds for HOMO-3 orbital for both the dyes are nonbonding combination localized on the NCS ligand. HOMO-4 and HOMO-5 orbitals of **MC**101 resemble those of corresponding orbitals of **C**101, in which π-clouds have

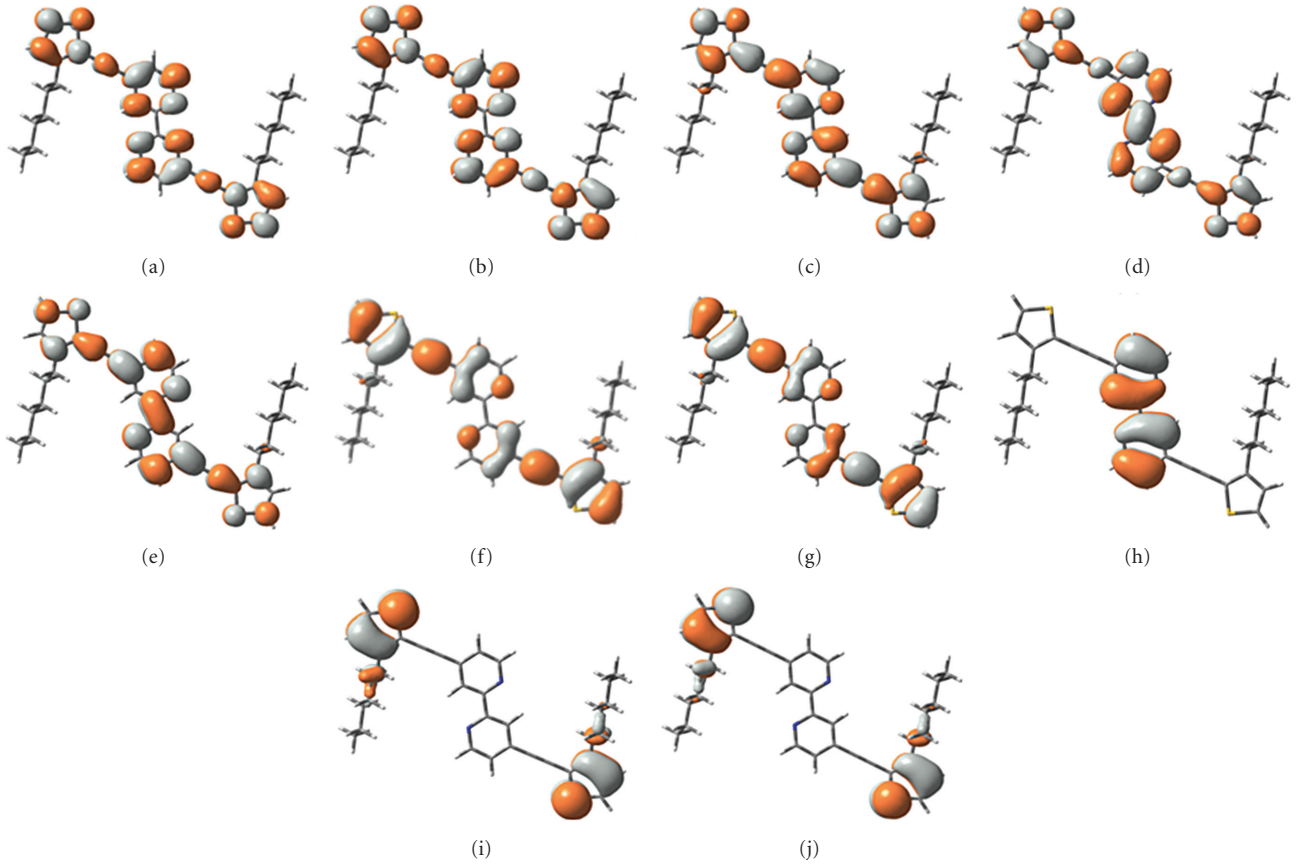

Figure 4: Frontier molecular orbitals of 4,4′-bis [(3-hexylthiophene)ethynyl]-2,2′-bipyridine: (a) LUMO+4, (b) LUMO+3, (c) LUMO+2, (d) LUMO+1, (e) LUMO, (f) HOMO, (g) HOMO-1, (h) HOMO-2, (i) HOMO-3, and (j) HOMO-4.

considerable mixing of Ru-NCS with π-bonding orbitals of 4,4′-bis [(3-hexyl thiophene)ethynyl]-2,2′-bipyridine (**L**1) in **MC**101 complex and 4,4′-bis(5-hexylthiophen-2-yl)-2,2′-bipyridine in **C**101 complex. In HOMO and HOMO-1 orbitals of the new ancillary bipyridine ligand, **L**1, the π-orbitals are more delocalized over the π-system and bipyridine, and this favorably lifted their energy levels. As it is seen in the electronic absorption spectrum of **MC**101, the absorption bands in UV-region corresponds to the π-π^* transitions of bipyridyl ligands, in which the **L**1 metalation with ruthenium(II) increased the spectral response of the complex along with bathochromic shift. The introduction of acetylene as extended π-conjugation resulted in a slight increase in the molar extinction coefficient of MLCT absorption band, which could be probably due to lifting their occupied molecular orbitals energy levels as compared to those of **C**101. Similar to LUMO of **C**101, the electron distribution in LUMO of **MC**101 moves toward the anchoring groups; while assuming similar molecular orbital geometry when adsorbed on TiO_2 surface, the close position of the LUMO to the anchoring moieties is expected to enhance the overlap with the 3d orbitals of TiO_2 leading to favored electron injection. In case of higher unoccupied molecular orbitals of the ancillary bipyridyl ligand, **L**1, the π^*-orbitals move from π-system to bipyridine moieties, and these transfers in **MC**101 significantly depress the LUMO+3 and LUMO+4 orbitals and a moderate extending in case of LUMO+1 orbital relative to those of **C**101. The calculated dipole moment for **MC**101 is 28.7. Debye is larger as compared to that of **C**101 (18.2 Debye). The increased dipole moment in gaseous phase signifies the formation of nearly stable geometry and facilitates better charge transfer for **MC**101 as compared to **C**101.

2.4. Thermal Stability. Although a very good conversion efficiency was obtained, the introduction of –C≡C– acetylene groups through 4,4′-bis(5-hexylthiophen-2-yl)-2,2′-bipyridine in **MC**101 complex may severely influence the thermal stability relative to **C**101 sensitizer. Hence the TGA analysis of **L**1, **L**2, and the corresponding ruthenium(II) complexes was performed using a TGA/SDTA 851^e thermal system (Mettler Toledo, Switzerland) at heating rate of 10°C/min in the temperature range of 25–600°C under N_2 atmosphere (flow rate of 30 mL/min). Film samples ranging from 8 to 10 mg were placed in the sample pan and heated, while weight losses are recorded against temperature difference. The thermograms of **MC**101 and **C**101 dyes are shown in (Figure 7), in which the derivative of % conversion plotted against temperature. The thermograms show gradual

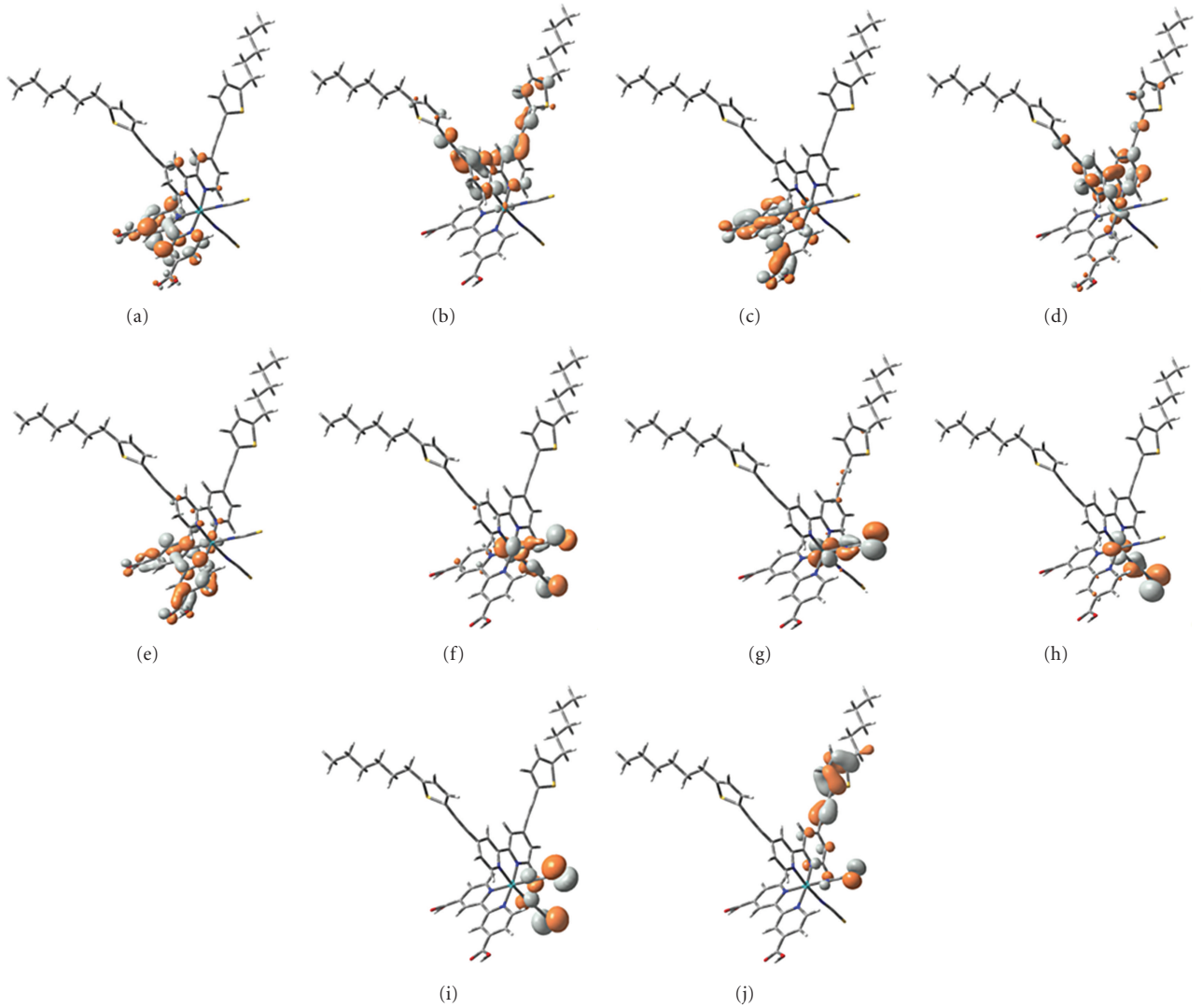

Figure 5: Frontier molecular orbitals of **MC**101: (a) LUMO+4, (b) LUMO+3, (c) LUMO+2, (d) LUMO+1, (e) LUMO, (f) HOMO, (g) HOMO-1, (h) HOMO-2, (i) HOMO-3, and (j) HOMO-4.

decomposition of **MC**101 complex as compared to **C**101, while the ligands are thermally stable.

2.5. Photovoltaic Properties. To evaluate the influence of 4,4′-bis(5-hexylthiophen-2-yl)-2,2′-bipyridine on the photovoltaic performance of DSSC, a high-quality double-layer titania films (9 + 4.8 μm) were employed to fabricate 0.54 cm^2 active area DSSC test cells in combination with a high performance electrolyte, (**E**01) containing 0.05 M I_2, 0.1 M LiI, 0.6 M 1,2-dimethyl-3-*n*-propylimidazolium iodide, and 0.5 M 4-*tert*-butylpyridine in acetonitrile solvent. The fabrication and evaluation of DSSC test cells were in accordance with the procedures reported [22]. Photon-to-current conversion efficiency spectrum was recorded as a function of excitation wavelength using a 300 W xenon lamp (ILC Technology, USA), which was focused through a Gemini-180 double monochromator (Jobin Yvon Ltd.). The incident photon-to-current conversion efficiency (IPCEs) of the DSSC constructed based on this dye is shown in Fig- ure 8(a). The monochromatic incident photon-to-collected electron conversion efficiency of 44.1% was obtained for over the entire visible range, which is less than unity suggesting a low charge collection yields. Under comparable conditions, **C**101 exhibited IPCE value of 40.1%. The photo current-voltage measurements were executed under Air Mass (AM) of 1.5 sunlight, and the the typical current density versus voltage curve is shown in Figure 8(b). The energy conversion efficiency of 3.25% (short-circuit current density (J_{SC}) = 7.32 mA/cm^2, V_{OC} = 610 mV, ff = 0.725) was obtained for **MC**101 sensitizer, while under comparable conditions, **C**101 exhibited conversion efficiency of 2.94%(J_{SC}) = 6.60 mA/cm^2, V_{OC} = 630 mV, and ff = 0.709) under Air Mass of 1.5 sunlight.

3. Conclusions

The new **MC**101 sensitizer with a new ancillary bipyridine ligand has several advantages. (1) Thiophene is a

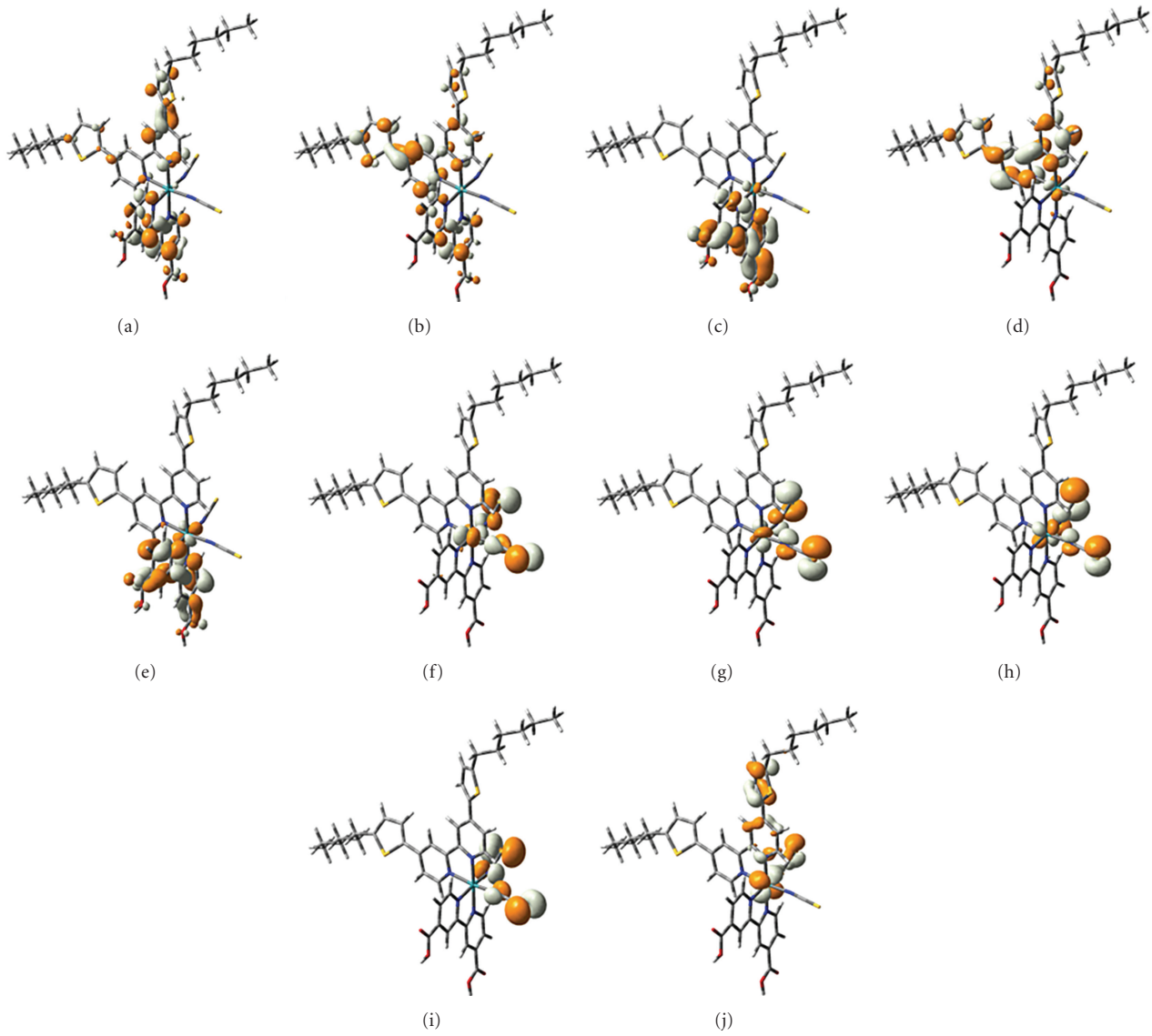

Figure 6: Frontier molecular orbitals of **C**101: (a) LUMO+4; (b) LUMO+3; (c) LUMO+2; (d) LUMO+1; (e) LUMO; (f) HOMO; (g) HOMO-1; (h) HOMO-2; (i) HOMO-3; (j) HOMO-4.

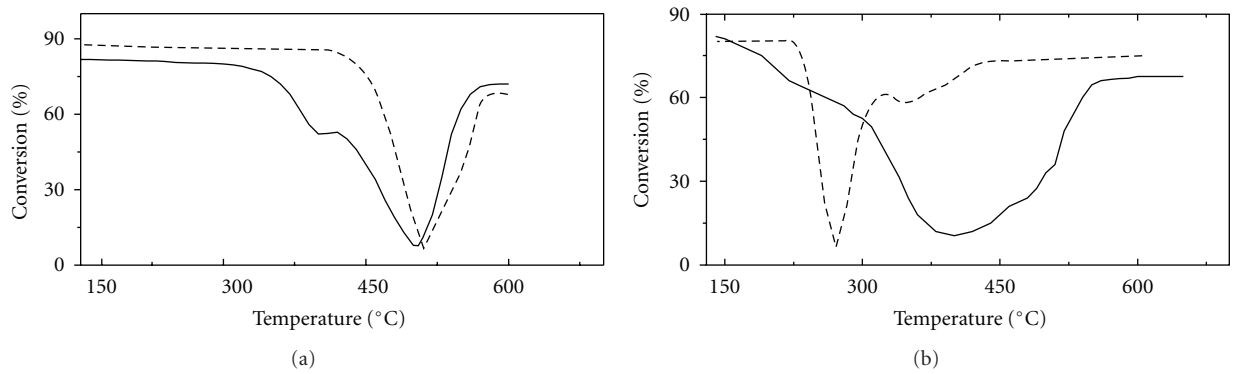

Figure 7: TG-Thermograms of (a) **L**1 (—) and **L**2 (- - -), (b) corresponding **MC**101 (—) and **C**101(- - -) complexes.

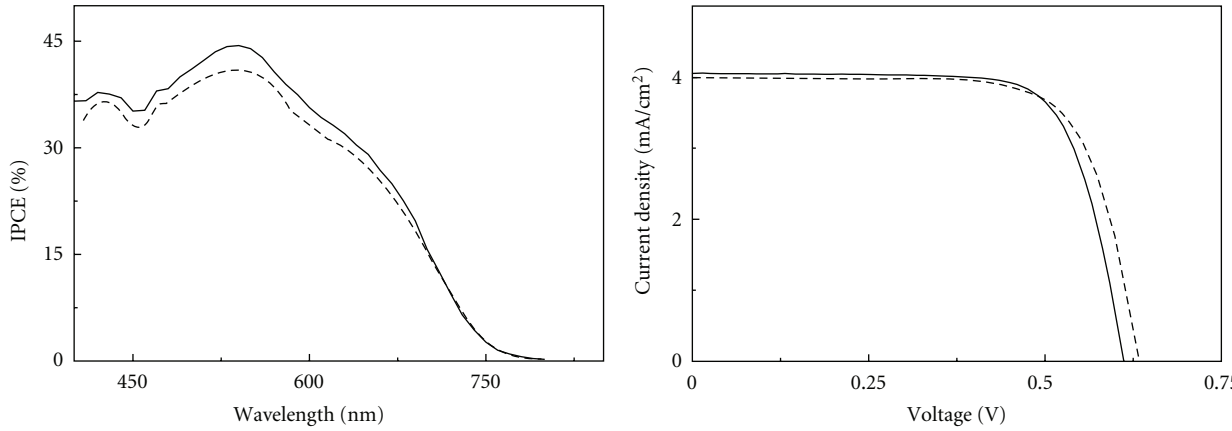

Figure 8: (a) Photocurrent action spectra of DSSC constructed based on **MC**101 sensitizer fabricated with **E**01 electrolyte; (b) corresponding *J- V* characteristics, measured under an irradiance of 100 mWcm^{-2} AM1.5G sun light.

more electron-rich moiety; incorporation of thiophene onto bipyridine ligands can raise the energy levels of the metal center and the LUMO of the ligands. (2) Facile functionalization of thiophene groups also offers relatively efficient synthetic solutions to solubility, polarity, and band-gap tuning. (3) The alkynyl thiophene can be considered as bis-acetylene moiety, where one acetylene is bridged with sulfur atom effectively providing aromatic stability while other free acetylene helps in the extension of conjugation for red shifting the absorption as well as increasing the molar extinction coefficient. Thus **MC**101 showed higher molar extinction coefficient combined with red shift in absorption and comparable performance with **C**101 sensitized solar cells, fabricated and evaluated under similar conditions. The TG analysis showed relatively decreased thermal stability for **MC**101 as compared to **C**101.

Acknowledgments

T.Suresh thanks CSIR, New Delhi for senior research fellowship. M.Chandrasekharam thanks DST, New Delhi for the grant of the project entitled "Efficient Solar Cells based on Organic and hybrid Technology (**ESCORT**)" under EU-DST consortium.

References

[1] M. D. Archer and R. Hill, *Clean Electricity from Photo Voltaics*, Imperical College Press, London, UK, 2001.

[2] Special issue on organic-based photovoltaics, *MRS Bulletin*, vol. 30, no. 1, pp. 10–53.

[3] A. Hagfeldt, G. Boschloo, L. Sun, L. Kloo, and H. Pettersson, "Dye-sensitized solar cells," *Chemical Reviews*, vol. 110, no. 11, pp. 6595–6663, 2010.

[4] B. O'Regan and M. Grätzel, "A low-cost, high-efficiency solar cell based on dye-sensitized colloidal TiO_2 films," *Nature*, vol. 353, no. 6346, pp. 737–740, 1991.

[5] M. Grätzel, "Photoelectrochemical cells," *Nature*, vol. 414, no. 6861, pp. 338–344, 2001.

[6] M. K. Nazeeruddin, F. De Angelis, S. Fantacci et al., "Combined experimental and DFT-TDDFT computational study of photoelectrochemical cell ruthenium sensitizers," *Journal of the American Chemical Society*, vol. 127, no. 48, pp. 16835–16847, 2005.

[7] Y. Chiba, A. Islam, Y. Watanabe, R. Komiya, N. Koide, and L. Han, "Dye-sensitized solar cells with conversion efficiency of 11.1%," *Japanese Journal of Applied Physics Part 2*, vol. 45, no. 24-28, pp. L638–L640, 2006.

[8] P. Wang, S. M. Zakeeruddin, J. E. Moser, M. K. Nazeeruddin, T. Sekiguchi, and M. Grätzel, "A stable quasi-solid-state dye-sensitized solar cell with an amphiphilic ruthenium sensitizer and polymer gel electrolyte," *Nature Materials*, vol. 2, no. 6, pp. 402–407, 2003.

[9] P. Wang, S. M. Zakeeruddin, R. Humphry-Baker, J. E. Moser, and M. Grätzel, "Molecular-scale interface engineering of TiO_2 nanocrystals: improving the efficiency and stability of dye-sensitized solar cells," *Advanced Materials*, vol. 15, no. 24, pp. 2101–2104, 2003.

[10] P. Wang, C. Klein, R. Humphry-Baker, S. M. Zakeeruddin, and M. Grätzel, "A high molar extinction coefficient sensitizer for stable dye-sensitized solar cells," *Journal of the American Chemical Society*, vol. 127, no. 3, pp. 808–809, 2005.

[11] P. Wang, Ć. Klein, R. Humphry-Baker, S. M. Zakeeruddin, and M. Grätzel, "Stable ≥ 8% efficient nanocrystalline dye-sensitized solar cell based on an electrolyte of low volatility," *Applied Physics Letters*, vol. 86, no. 12, Article ID 123508, pp. 1–3, 2005.

[12] D. Kuang, C. Klein, S. Ito et al., "High effiiciency and stable mesoscopic dye-sensitized solar cells based on a high molar extinction cofficient Ru-sensitizer and non-volatile electrolyte," *Advanced Materials*, vol. 19, pp. 1133–1137, 2007.

[13] J. R. Durrant and S. A. Haque, "Solar cells: a solid compromise," *Nature Materials*, vol. 2, no. 6, pp. 362–363, 2003.

[14] P. Wang, S. M. Zakeeruddin, J. E. Moser et al., "Stable new sensitizer with improved light harvesting for nanocrystalline dye-sensitized solar cells," *Advanced Materials*, vol. 16, no. 20, pp. 1806–1811, 2004.

[15] K. J. Jiang, N. Masaki, J. B. Xia, S. Noda, and S. Yanagida, "A novel ruthenium sensitizer with a hydrophobic 2-thiophen-2-yl-vinyl- conjugated bipyridyl ligand for effective dye sensitized TiO_2 solar cells," *Chemical Communications*, no. 23, pp. 2460–2462, 2006.

[16] S. R. Jang, C. Lee, H. Choi et al., "Oligophenylenevinylene-functionalized Ru(II)-bipyridine sensitizers for efficient dye-sensitized nanocrystalline TiO_2 solar cells," *Chemistry of Materials*, vol. 18, no. 23, pp. 5604–5608, 2006.

[17] C. Y. Chen, S. J. Wu, C. G. Wu, J. G. Chen, and K. C. Ho, "A ruthenium complex with superhigh light-harvesting capacity for dye-sensitized solar cells," *Angewandte Chemie International Edition*, vol. 45, no. 35, pp. 5822–5825, 2006.

[18] C. S. Karthikeyan, H. Wietasch, and M. Thelakkat, "Highly efficient solid-state dye-sensitized TiO_2 solar cells using donor-antenna dyes capable of multistep charge-transfer cascades," *Advanced Materials*, vol. 19, no. 8, pp. 1091–1095, 2007.

[19] C. Y. Chen, S. J. Wu, J. Y. Li, C. G. Wu, J. G. Chen, and K. C. Ho, "A new route to enhance the light-harvesting capability of ruthenium complexes for dye-sensitized solar cells," *Advanced Materials*, vol. 19, no. 22, pp. 3888–3891, 2007.

[20] F. Gao, Y. Wang, D. Shi et al., "Enhance the optical absorptivity of nanocrystalline TiO_2 film with high molar extinction coefficient ruthenium sensitizers for high performance dye-sensitized solar cells," *Journal of the American Chemical Society*, vol. 130, no. 32, pp. 10720–10728, 2008.

[21] M. Chandrasekharam, C. Srinivasarao, T. Suresh et al., "High spectral response heteroleptic ruthenium (II) complexes as sensitizers for dye sensitized solar cells," *Journal of Chemical Sciences*, vol. 123, no. 1, pp. 37–46, 2011.

[22] M. Chandrasekharam, G. Rajkumar, C. S. Rao, T. Suresh, and P. Y. Reddy, "Phenothiazine conjugated bipyridine as ancillary ligand in Ru(II)-complexes for application in dye sensitized solar cell," *Synthetic Metals*, vol. 161, no. 15-16, pp. 1469–1476, 2011.

[23] P. Y. Reddy, L. Giribabu, C. Lyness et al., "Efficient sensitization of nanocrystalline TiO_2 films by a near-IR-absorbing unsymmetrical zinc phthalocyanine," *Angewandte Chemie International Edition*, vol. 46, no. 3, pp. 373–376, 2007.

[24] L. Giribabu, M. Chandrasekheram, M. L. Kantham et al., "Conjugated organic dyes for dye-sensitized solar cells," *Indian Journal of Chemistry Section A*, vol. 45, no. 3, pp. 629–634, 2006.

[25] M. Chandrasekharam, G. Rajkumar, C. Srinivasa Rao et al., "Polypyridyl Ru(II)-sensitizers with extended π-system enhances the performance of dye sensitized solar cells," *Synthetic Metals*, vol. 161, no. 11-12, pp. 1098–1104, 2011.

[26] L. Giribabu, C. Vijay Kumar, C. S. Rao et al., "High molar extinction coefficient amphiphilic ruthenium sensitizers for efficient and stable mesoscopic Dye-sensitized solar cells," *Energy and Environmental Science*, vol. 2, no. 7, pp. 770–773, 2009.

[27] L. Han, A. Islam, H. Chen et al., "High-efficiency dye-sensitized solar cell with a novel co-adsorbent," *Energy and Environmental Science*. In press.

[28] J. J. Cid, J. H. Yum, S. R. Jang et al., "Molecular cosensitization for efficient panchromatic dye-sensitized solar cells," *Angewandte Chemie International Edition*, vol. 46, no. 44, pp. 8358–8362, 2007.

[29] D. Kuang, C. Klein, S. Ito et al., "High molar extinction coefficient ion-coordinating ruthenium sensitizer for efficient and stable mesoscopic dye-sensitized solar cells," *Advanced Functional Materials*, vol. 17, no. 1, pp. 154–160, 2007.

[30] B. S. Chen, K. Chen, Y. H. Hong et al., "Neutral, panchromatic Ru(ii) terpyridine sensitizers bearing pyridine pyrazolate chelates with superior DSSC performance," *Chemical Communications*, no. 39, pp. 5844–5846, 2009.